scientific reports

OPEN

Free-standing millimeter-range 3D waveguides for on-chip optical interconnects

Artur Andrishak, Bejoys Jacob, Tiago L. Alves, Christian Maibohm, Bruno Romeira & Jana B. Nieder ✉

Next-generation energy-efficient photonic integrated systems, such as neuromorphic computational chips require efficient heterogeneous integration of ultracompact light sources and photodetectors through highly dense waveguide circuits. However, interconnecting these devices in emitter-receiver communication circuits remains a challenge and an obstacle towards upscaling heterogeneous photonic chips. Here we report on versatile air-cladded free-standing 3D polymer waveguides (OrmoCore, n≈1.5) spanning up to 900 µm in length without intermediate mechanical support structures, microprinted via two-photon polymerization. The presented waveguides are suitable for on-chip out-of-plane light coupling as well as non-connected 3D crossings, needed for high density optical circuits. The waveguides show optical transmission losses of 1.93 dB mm^{-1} at λ = 635 nm, and of 3.71 dB mm^{-1} at λ = 830 nm in the wavelength range of GaAs-based microLEDs spectral emission. On-chip imaging for high-precision alignment and TPP microfabrication are performed seamlessly by utilizing the same laser source for both steps, allowing accurate 3D printing on microstructured substrates. As proof of concept, we interconnect two GaAs-based microLEDs via an on-chip microprinted 3D waveguide. Such combined systems can serve as building blocks of future complex integrated heterogeneous photonic networks.

Waveguide-based optical interconnects represent a promising platform for achieving on-chip communication between compact integrated light-generating, and detecting devices, constituting an important milestone towards the realization of neuromorphic computational and quantum photonic platforms[1,2]. Recent advancements in photonic devices for light-based communication and neuromorphic computing have demonstrated high operation speed and energy efficiency[3]. Notable examples include III–V/Si integrated spiking nanoscale light emitting diodes (LEDs) integrated with resonant tunneling diodes[4], nanolaser diodes[5], graphene excitable lasers[6] vertical-cavity surface-emitting lasers (VCSELs)[7], and III-V nanowire LEDs[8], many of which feature vertical emission profiles. Despite these advances, integration of these novel photonic devices into emitter-receiver communication circuits using planar optical waveguides remains challenging. For instance, III-V emitter devices based on semiconductor nanowires require highly precise pick-and-place technology or micro-transfer printing processes to position them on prefabricated photonic circuits containing waveguides, thus presenting significant alignment challenges[9,10]. Additionally, devices such as nanoLED and nanolaser pillars require vertical out-of-plane light coupling into the photonic circuit[11]. Recent realizations of such configurations estimate coupling efficiencies of 29% for an ideal nanoLED pillar and 7% for a pillar with sloped sidewalls[12]. Moreover, upscaling complex interconnected networks with a high number of input–output (IO) channels while maintaining a small chip footprint is particularly challenging with 2D lithography techniques due to disadvantageous scaling. In fact, the footprint of 2D interconnect networks grows quadratically with the number of IO channels, as evidenced by architectures such as crossbar arrays[13]. Other established technologies for photonic interconnects include the use of optical fibers which have very low optical propagation losses but suffer from limited coupling efficiencies due to the NA of the fiber or mismatch between off-chip fiber core and on-chip waveguide core sizes potentially leading to high losses[14]. Reducing these losses typically requires the fabrication of polymer tapered structures[15] or microlenses[16] on the device to be interconnected or directly on the optical fiber. Additionally, the large cladding of optical fibers makes on-chip and inter-chip integration more difficult.

Alternatively, two-photon polymerization (TPP) offers significant advantages over standard planar UV lithography. TPP allows direct on-chip microprinting of three-dimensional (3D) waveguides with complex geometries that facilitate out-of-plane light routing. This capability eliminates the need for micro- and nanophotonic

INL - International Iberian Nanotechnology Laboratory, Ultrafast Bio- and Nanophotonics Group, Av. Mestre Veiga, s.n., 4715–330 Braga, Portugal. ✉email: jana.nieder@inl.int

device transfer onto prefabricated waveguide circuits. The TPP technique has been successfully employed in a wide range of optical applications including the fabrication of optical fiber tapers[17], beam shaping structures[18], microlenses[19–21], beam splitters[22,23], photonic crystals[24], and circuits for nitrogen-vacancy quantum photonics[25]. Previous studies utilizing TPP have demonstrated the successful microprinting of low loss buried optical waveguides, via laser-induced localized changes in refractive index within pre-cured polymer slabs, such as polymethyl methacrylate (PMMA)[26] and polydimethylsiloxane (PDMS)[27]. Such waveguides have achieved a refractive index contrast in the range of 10^{-3}-10^{-2}. However, this refractive index contrast results in insufficient light confinement for fabricating waveguides with sharp bends, which may be necessary to minimize the physical footprint of complex interconnect networks. To address these limitations, air-cladded free-form 3D waveguides with a higher refractive index contrast between core and cladding ($\Delta n \approx 0.5$) have been demonstrated via TPP in complex neural network configurations, albeit with higher optical propagation losses of 20 dB mm^{-1}[28]. A particularly interesting application of TPP is photonic wire bonding (PWB). Free-standing 3D waveguides with core diameters of less than 2 μm spanning lengths of more than 100 μm have been successfully microprinted via TPP to interconnect nanophotonic circuits, achieving total insertion losses as low as 1.6 dB in the C-band and Tbit/s data transmission[29]. Fiber-to-chip 3D waveguides have been demonstrated with similar insertion losses[30], as well as similar waveguides interconnecting InP lasers with silicon photonic circuits with insertion losses of only 0.4 dB[31]. However, millimeter-range 3D free-standing waveguides have been successfully demonstrated via TPP only with the assistance of multiple intermediate mechanical support structures[32–34]. These supports can increase optical propagation losses due to scattering and unwanted light outcoupling from the waveguide core to the supports and complicate 3D superposition of crossing waveguides, therefore limiting interconnect integration density. Marschner et al. successfully demonstrated a methodology to microprint millimeter-range overhanging polymer structures via TPP using Nanoscribe's IP-S resin, wherein a long straight 3D object is subdivided into blocks of smaller volume, preventing the larger structure from floating during fabrication[35]. Here, we adopt a similar concept but instead of subdividing the waveguide design into smaller 3D blocks, we employ a single continuous line as the voxel trajectory to polymerize millimeter-range arched 3D waveguides. The development of millimeter-range free-standing 3D waveguides will enable the upscaling of photonic neuromorphic systems by facilitating interconnections between different large-scale system sub-circuits.

In this work, we present the development of 3D free-standing waveguides fabricated via TPP in OrmoCore without intermediate support structures. We successfully microprinted long 3D waveguides in OrmoCore up to 900 μm in length without any intermediary structures, surpassing previous limitations for this polymer[34]. OrmoCore is selected as damage threshold is expected to be appropriate for the intended application to optically interconnect micro light sources. This polymer is optically transparent in the visible and near-infrared ranges, it is stable even at temperatures of 150 °C long term and up to 270° C short term exposure (as specified by material provider). We demonstrate vertical 3D superposition of waveguides without unwanted core intersections, enabling higher density of interconnects. Furthermore, our waveguides exhibit out-of-plane light rerouting capabilities and favorable optical propagation properties, with losses comparable to state-of-the-art 3D waveguides fabricated via TPP (for a more detailed comparison see Table S1 in supplemental document section S8), making them suitable candidates for on-chip optical interconnects. As a proof-of-concept, we fabricated 3D waveguides directly on a GaAs semiconductor-based photonic chip, successfully achieving optical interconnection between two microLEDs operating in an emitter-receiver configuration for the first time. These systems have the potential to form the basis for the implementation of photonic artificial neurons, which are essential building blocks of neuromorphic computing systems.

Results

We design arched 3D waveguides consisting of two main parts: i) inclined tapers at each end, and ii) an arched waveguide core with a straight middle section for linear optical propagation (Fig. 1a). The waveguide core is microprinted using a continuous zig-zag voxel trajectory where the lateral width of the waveguide is polymerized first, followed by an incremental polymerization along the waveguide's length (Fig. 1b). The tapers are polymerized in concentric circles from the bottom up (Fig. 1c). This fabrication method ensures that the 3D structures are structurally resistant to the rapid movement of the high-precision translational piezo stage (nano-stage) which follows the specified 3D voxel trajectories. For structures exceeding the maximum range of the nano-stage (200 μm), the stitching process is performed successfully using a micro-step motor stage (micro-stage). Any potential misalignment resulting from the repositioning of the micro-stage is pre-compensated in the 3D voxel trajectory, ensuring accurate microprinting.

Our approach enabled the fabrication of microprinted 3D waveguides with lengths up to 900 μm with no intermediate support structures, achieved by performing successive stitching steps. The design and fabrication parameters used are a zig-zag trajectory with period T = 1 μm (resulting in a 500 nm hatching distance between parallel lines), nano-stage movement speed v = 100 μm s^{-1} and laser fluence values of F = 16.5 mJ cm^{-2} for the waveguide cores and 19.8 mJ cm^{-2} for the tapers. Choosing a higher laser fluence for the polymerization of vertical tapers permits the use of a larger hatching distance, reducing the overall printing time. Conversely, a lower laser fluence is used for the waveguide core to limit its vertical polymerization extent. The resulting rounded rectangular waveguide core size is, approximately, 9×33 μm^2, in the horizontal and vertical directions respectively. For further context, Figure S6 demonstrates that an alternative voxel trajectory, consisting of long parallel lines along the waveguiding direction, does not result in successful stitching of long structures, underscoring the importance of selecting an appropriate slicing and writing voxel trajectory to achieve optimal microprinting outcomes. Figure 2a displays a scanning electron microscopy (SEM) image of the fabricated 3D waveguides, and Fig. 2b presents the optical transmission losses plotted against the waveguide length for waveguides with a height of 44 μm, varying in length from 200 μm to 900 μm. A total of 24 waveguides were microprinted and
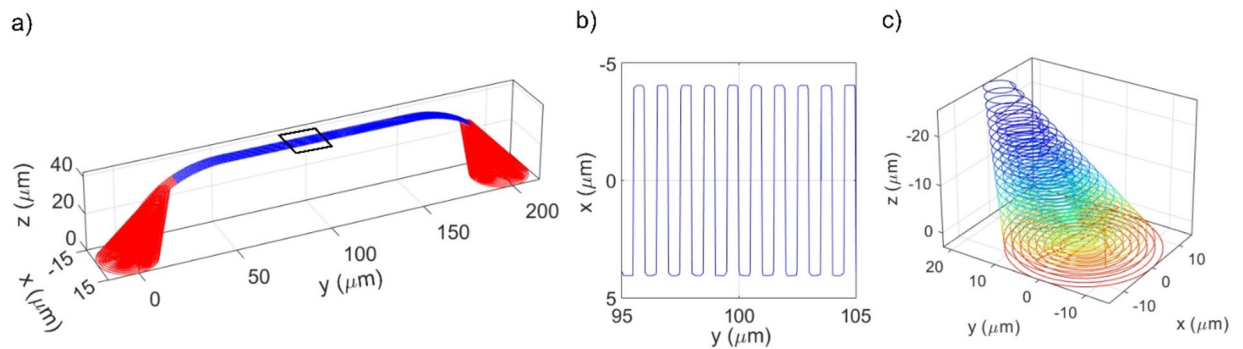
Figure 1. Voxel trajectory used to microprint the 3D waveguides. (**a**) 3D design of free-standing waveguide, consisting of two inclined tapers (red), and suspended air-cladded waveguide core (blue). See supplemental information section S5 for mathematical parametrization. (**b**) Zoomed-in top view of the waveguide core section with a voxel trajectory composed of a single continuous zig-zag line with a period of 1 μm, resulting in a hatching of 0.5 μm. (**c**) Cone-shaped 3D taper constructed by a voxel trajectory composed of concentric circles stacked together, where $R_{max} = 15$ μm and $R_{min} = 4$ μm, vertical hatching distance $d_z = 1.5$ μm and horizontal hatching $d_{xy} = 1.5$ μm. The colors represent the order of microprinting: from red to blue.
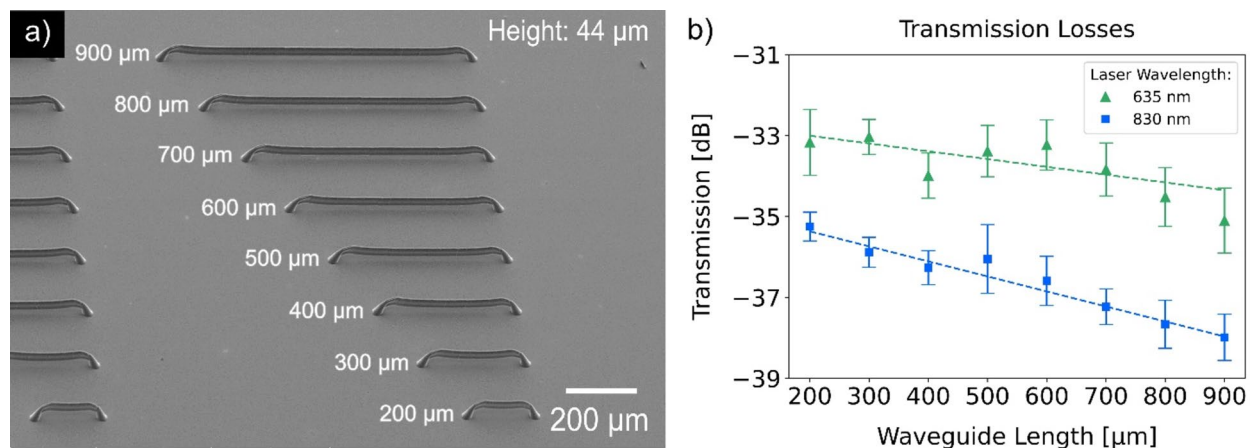
Figure 2. (**a**) SEM image of microprinted waveguides with height 44 μm, with lengths ranging from 200 to 900 μm and printing parameters: zig-zag period T = 1 μm, laser fluence F = 16.5 mJ cm^{-2} for the waveguide core and F = 19.8 mJ cm^{-2} for the tapers, and stage movement velocity v = 100 μm s^{-1}. (**b**) Plot of optical transmission vs waveguide length at different characterization wavelengths. The propagation losses are 1.93 ± 0.73 dB mm^{-1} and 3.71 ± 0.27 dB mm^{-1} at λ = 635 nm and λ = 830 nm, respectively.

characterized using a custom-built optical setup (described in the Materials and Methods section, and in more detail in supplemental document section S4). Two laser wavelengths, 635 nm and 830 nm, were employed for optical transmission measurements. The laser light is coupled through the transparent substrate to one taper of each waveguide using a microlensed optical fiber, and the output intensity at the opposite end of the waveguide was recorded with a sCMOS camera. The measured optical propagation losses are 1.93 ± 0.73 dB mm^{-1} at 635 nm and 3.71 ± 0.27 dB mm^{-1} at 830 nm. Additionally, waveguides with a height of 76 μm were also microprinted; however they presented a high degree of bending which further increased the propagation losses (Figure S7).

The optical propagation losses can be attributed to scattering resulting from surface defects and uneven texture of the structures. The surface roughness of the structures is caused by the hatching distance of the design and it is on the same order of magnitude as the characterization wavelengths. We performed 3D FDTD and MODE solver simulations in Lumerical to assess the scattering effect near the waveguide sidewalls. We use a high fidelity 3D model of our waveguides that includes a surface roughness with 500 nm period caused by the hatching distance of the voxel trajectory. We obtain this model using a TPP shape prediction tool developed by us which takes into account experimental microprinting parameters, material characteristics and 3D voxel trajectory (more details in Ricardo Adão et al.[34]). The fundamental TM mode is used as an input source at the taper base, and an electric field monitor is placed at the cross-section of the waveguide after the bend, showing the multimode character of the waveguide (Fig. 3a). We then perform a more detailed simulation using a finer mesh to accurately resolve the sub-micrometer sidewall roughness and assess the effect of light scattering at these boundaries. We perform this simulation by propagating the fundamental TM mode and an arbitrary high order mode ($n_{eff} \approx 1.4$, Fig. 3b) for a distance of 7 μm in the waveguiding direction corresponding to the y-axis. The results for the scattering simulations are plotted on the same logarithmic scale and show that there
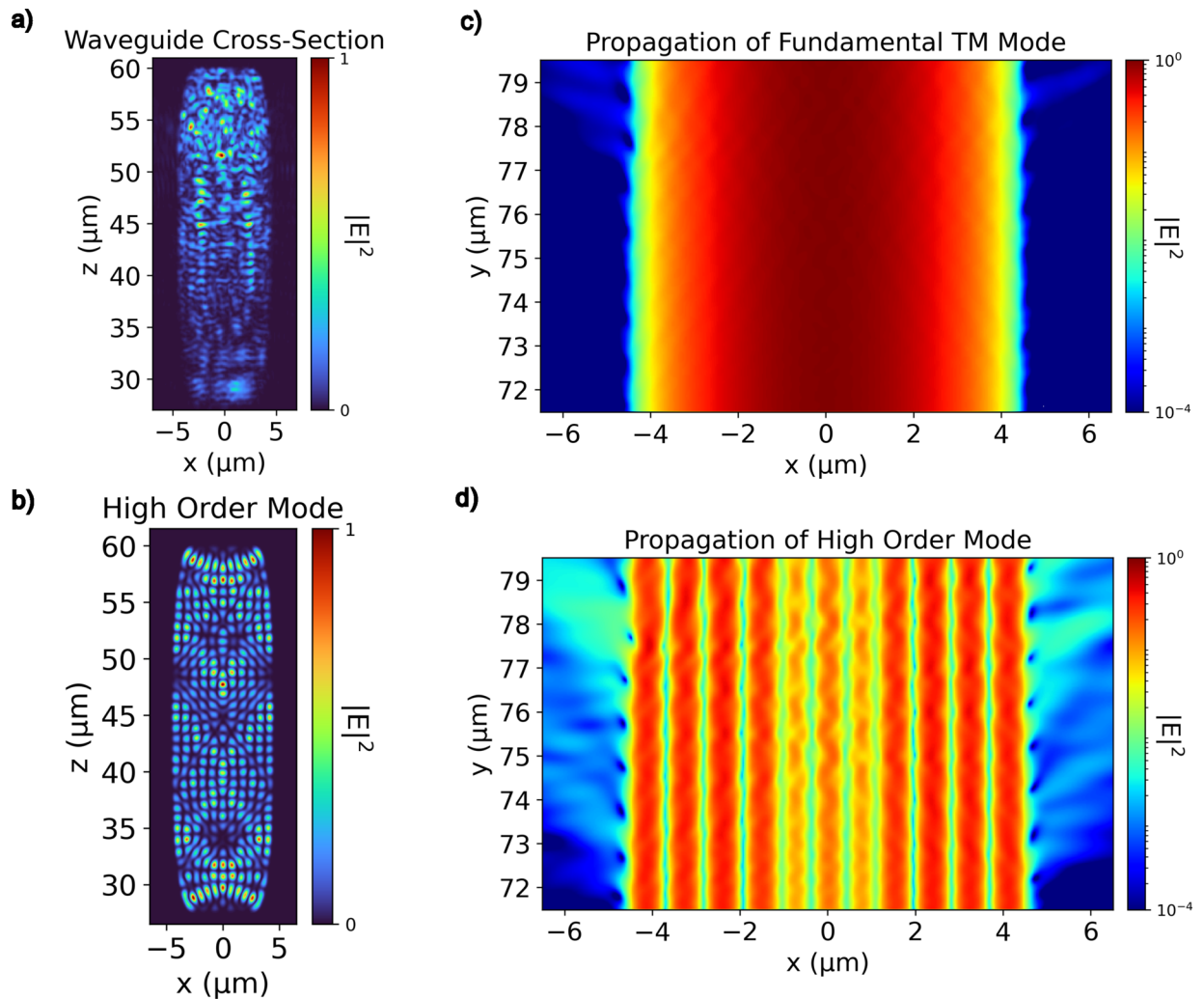
Figure 3. 3D FDTD and MODE solver simulations of mode field propagation in the 3D waveguide. (**a**) Multimode profile at waveguide cross-section after propagating the fundamental TM mode from the waveguide taper. The source emits at an angle of 15° similar to the optical fiber used in the characterization setup. (**b**) Waveguide cross-section with arbitrary high order mode ($n_{eff} \approx 1.4$) chosen to assess the effect of multimode propagation on scattering losses due to surface defects of the waveguide. It is this mode that is propagated in (**d**). (**c**) FDTD simulation of the fundamental TM mode propagating through the center of the waveguide at a height of approximately 44 μm. The scattering from the sidewalls can be seen increasing with propagation distance. (**d**) FDTD simulation of a high order mode mode propagating through the center of the waveguide showing increased scattering from the sidewalls compared to the fundamental TM mode propagation. The simulations are performed at a wavelength $\lambda = 830$ nm.

is a significantly higher degree of scattering from the waveguide sidewalls in the propagation of the high order mode (Fig. 3d) compared to the fundamental TM mode (Fig. 3c). The high order mode presents an optical power distribution that extends to the waveguide sidewalls, making high order modes more prone to scattering due to surface defects and roughness. Single-mode operation for air-cladded OrmoCore waveguides can be achieved for a rounded-square core cross-section of side length equal to 510 nm at $\lambda = 830$ nm, and 390 nm at $\lambda = 635$ nm, according to Lumerical MODE solver simulations. Such core dimensions for millimeter-range free-standing waveguides are difficult to achieve with TPP microprinting due to compromised structural stability. Alternatively, single-mode operation can be achieved while maintaining larger waveguide core dimensions by reducing the refractive index contrast between core and cladding. For example, a cladding material with a slightly lower refractive index can be added in a second TPP microprinting step. The same effect can be achieved within the same material in a single fabrication step by exposing the core and cladding areas with different laser exposure doses as demonstrated by Porte et al.[36]. However, for lower speed TPP microprinting setups, exposing the waveguide with additional voxel trajectories to polymerize separately the core and cladding can potentially lead to even larger structure elongation.

The elimination of intermediate support structures renders the presently reported waveguides more suitable for the implementation of compact neuromorphic networks. These networks benefit from the capability to integrate a high density of interconnects through non-interacting crossing waveguides. To demonstrate this

capability, two 180 μm long waveguides of different heights crossing at the center at an angle of approximately 50° were microprinted, as depicted in Fig. 4. The fabrication sequence involved printing the higher waveguide first to prevent distortion of the laser beam by a polymerized waveguide with lower height. The square-wave voxel trajectory period T is set to 0.3 μm, and a reduced laser fluence of 8.8 mJ cm^{-2} for the waveguide core printing allowed for a reduction in vertical elongation of the waveguide core from 33 μm to 28 μm. The stage movement speed and the laser fluence used for the taper polymerization were kept consistent with the previously presented waveguides. In this manner, we obtained a ~ 75 μm high waveguide crossing over a ~ 25 μm high waveguide without intersecting cores., This outcome demonstrates that the developed waveguide architecture and TPP voxel trajectory enable the microprinting of multiple stacked suspended waveguides with 3D geometries, thereby allowing a higher integration density of optical interconnects.

Micro- and nanopillar LEDs can be designed for efficient light extraction and constitute a suitable platform to test the efficacy of the 3D suspended waveguides developed in this work for enabling on-chip interconnections between active photonic devices. Here, we optically interconnect two pairs of micropillar pin-type LEDs, with micropillar diameters of 12 μm and 14 μm. These LEDs feature a GaAs bulk emitter on a semi-insulating GaAs substrate and operate at a wavelength of approximately 860 nm, and are fabricated through a similar process as reported by Jacob et al[37]. Conducting TPP microprinting on opaque substrates, such as semiconductor dies, requires inverting the substrate and enclosing the polymer layer using a transparent coverglass and two spacers (Figure S2b). For alignment, the sample is imaged and aligned through the polymer layer without causing unwanted polymerization. To this effect, the fabrication laser fluence is decreased to F = 220 μJ cm^{-2}, which is below the polymerization threshold for OrmoCore. The laser is focused on the surface of the semi-insulating GaAs substrate containing the microLEDs. The laser then scans the surface of the substrate, and light intensity images based on the back-reflected light are recorded by an avalanche photodiode (APD). Figure 5a shows the resulting images of the microLEDs with good contrast which can be further enhanced by adjusting the photon count color scale. The substructures of the microLED are easily recognizable: the metal electrical contacts (brighter areas) that cover half of the circular pillar, and the GaAs substrate and light emitting circular pillar (darker regions). The imaging process is used to precisely center the fabrication laser focus on the center of the microLED structure with an accuracy of 1 μm. Structure dimensions in the recorded intensity images correspond to the microLED electron beam mask design. Considering this layout, 3D waveguides were designed to interconnect several pairs of microLEDs separated by a distance of 250 μm. After centering the fabrication laser on one of the circular micropillars, TPP microprinting of 3D waveguides is performed with the following printing parameters: the laser fluence for taper polymerization is slightly reduced to F = 18.7 mJ cm^{-2} due to laser reflection from the semiconductor substrate surface, and for the waveguide core a laser fluence F = 8.8 mJ cm^{-2} is used with a square-wave voxel trajectory of period T = 0.3 μm. For the electro-optical tests, a ground-signal-ground electrical probe was used to bias only one microLED from each pair up to 1.4 V, thereby triggering light emission. Figure 5b–d present camera images of the microLEDs interconnected via a 3D polymer waveguide. When biased to 1.4 V, a portion of the microLED light propagates through the waveguide, reaching the output microLED where it is scattered and recorded by the sCMOS camera. Figure 5e presents the 2D finite-difference time-domain (FDTD) simulation of light propagating through the suspended waveguide from a light source with angular emission similar to the used microLEDs. The 3D waveguide model accounts for defects in the tapers resulting from overexposure due to laser reflection from the substrate (see Figure S8 in supplemental information). Considering the taper losses calculated from the simulations (6.1 dB) and the experimental propagation losses at λ = 830 nm reported above (3.71 dB mm^{-1}), we estimate total optical losses of approximately 7 dB for the interconnected system, meaning that 20% of the input microLED light reaches the second device. Since the receiver LED was not designed to operate as a highly efficient photodiode, we were unable to measure the photocurrent resulting from the light received from the emitting microLED. Optical pulse broadening due
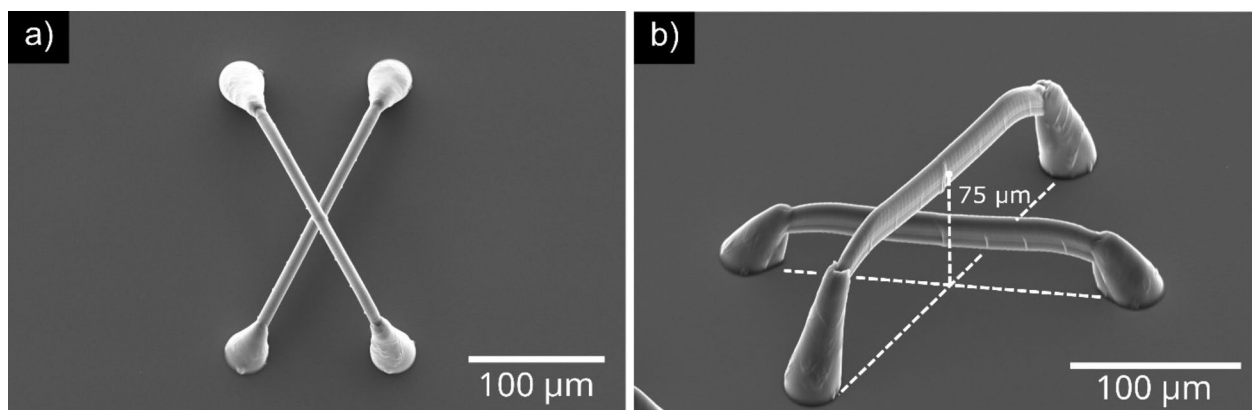
Figure 4. SEM images of crossing 3D waveguides. (**a**) Top view of a set of waveguides crossing at their center, making an angle of ~ 50° between them. Both waveguides are 180 μm long. (**b**) Tilted view of the set of crossing waveguides, the higher waveguide (height ~ 75 μm) is fabricated first and the second one (height ~ 25 μm) is fabricated last to avoid lensing effects of the laser beam. The resulting waveguides have a core size of, approximately, 9 × 28 μm². Printing parameters: zig-zag period T = 0.3 μm, laser fluence F = 8.8 mJ cm^{-2} for the waveguide core and F = 19.8 mJ cm^{-2} for the tapers, stage velocity v = 100 μm s^{-1}.
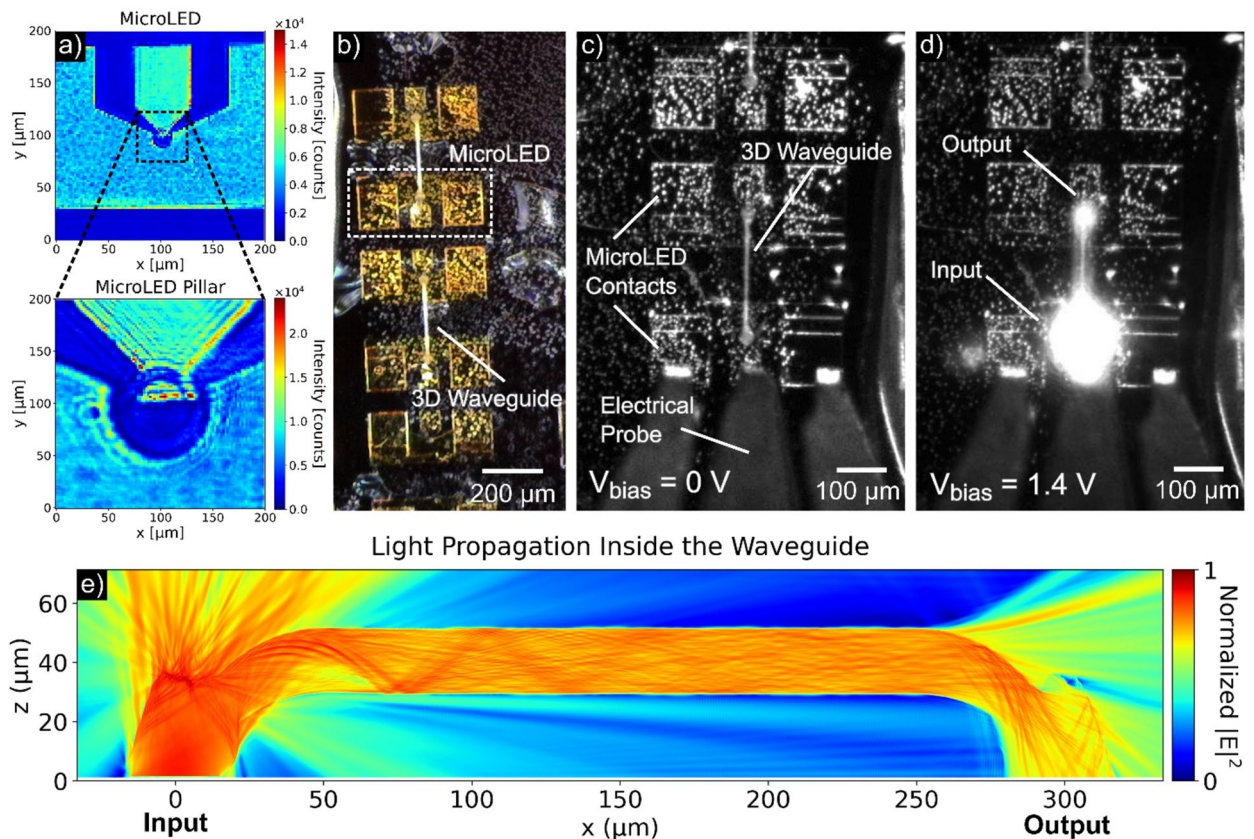
Figure 5. Interconnected microLEDs via a 3D polymer waveguide. (**a**) Back scattered light intensity images of a micro-ring LED with a diameter of 14 μm. Top and bottom images are zoomed out and zoomed in views, respectively. (**b**) Camera image of two 250 μm long waveguides, interconnecting two pairs of microLEDs facing each other. (**d**) SCMOS camera image of a 3D polymer waveguide, interconnecting a pair of microLEDs with a circular pillar 14 μm diameter, where the input microLED is biased at 0 V. (**d**) Input microLED biased at a voltage of 1.4 V via a ground-signal-ground electrical probe. The emitting light is coupled to the 3D waveguide, reaching the output at the second microLED. (**e**) 2D FDTD simulation of light propagating in an accurate model of a 3D waveguide microprinted on a GaAs semiconductor chip containing microLEDs. The simulation consider Gaussian sources varying in angle from −30° to 60° in relation to the substrate normal vector, and 10 wavelength points centered around 860 nm with a span of 35 nm, similar to the microLED emission. Simulation details can be consulted in supplemental document section S6 and a 2D FDTD simulation of a 3D waveguide without taper defects in Figure S5.

to intermodal dispersion can become a limitation on data transmission rates when interconnecting ultra-fast picosecond light sources with large-core multimode 3D waveguides[38]. Since microLEDs typically show optical signal modulation as short as 1 ns[37], optical pulse broadening does not compromise intercommunication between these devices via 3D multimode waveguides in the micro- and millimeter distance range. Future work will focus on integrating both a microLED and a highly efficient photodiode within the same epilayer stack to establish an emitter-receiver communication with 3D interconnectivity.

Conclusion

We demonstrated the importance of strategic voxel trajectory design to increase mechanical stability of TPP fabricated 3D structures. Specifically, by prioritizing the polymerization of the waveguide core's lateral width and incrementally increasing its length, the zig-zag voxel trajectory enables the printing of stable suspended structures capable of withstanding the rapid movement of the translational stages during the printing process. Notably, we have successfully fabricated mechanically challenging 3D structures, such as millimeter-range suspended waveguides, which had not been achieved in OrmoCore via TPP prior to this work. Thus, the presented strategy significantly improves the mechanical stability of TPP-printed 3D structures using materials that were previously thought to lack such mechanical robustness. Future improvements of the optical properties of microprinted 3D waveguides involve reducing surface roughness and optimizing the taper geometry and dimensions. Additionally, we demonstrated the compatibility between semiconductor photonics technology and the TPP process by developing laser-based alignment procedures and directly microprinting 3D interconnects on microstructured GaAs semiconductor-based photonic chips. The alignment procedure is levered by the laser fluence threshold required to trigger the TPP chain reaction, allowing the same laser source to be used both for imaging of microstructured substrates and for microprinting 3D structures. The seamless transition from

imaging the substrate through the polymer layer without causing polymerization to the microprinting step is achieved by simply adjusting the laser fluence, significantly simplifying the alignment process. This procedure proved to be successful in correctly identifying the microstructures' position and size, and aligning the laser at their center with an accuracy of 1 μm (accuracy of micro-step motor stage). The alignment process enabled us to create a proof-of-concept heterogeneous system consisting of two GaAs semiconductor-based microLEDs interconnected via a 3D OrmoCore waveguide. By electrically exciting one of the microLEDs, we demonstrated out-of-plane light routing from one microLED to the other via the 3D optical interconnect. We anticipate that the presented approach can be employed in inter-chip interconnects, and to interconnect not only micro light sources by detecting their positions through variations in reflectivity within the chip but also to interconnect nanoscale light sources or even single-photon emitters, such as single point defects in 2D materials, by collecting their emissions using detectors with high quantum efficiency in the alignment process.

The successful demonstration of free-standing and superimposed 3D waveguides on glass and on chip can establish such interconnects as fundamental building blocks for highly interconnected parallel photonic platforms, such as neuromorphic computational systems. Demonstration of precision alignment on microstructured chips containing microLEDs, and the subsequent microprinting of 3D interconnects represents a significant first step towards 3D heterogeneous integration.

Materials and methods
TPP printing and imaging setup
The custom TPP printing setup is based on a tunable Titan Sapphire femtosecond laser (Tsunami, Spectra Physics) tuned to a wavelength of 740 nm, with a repetition rate of 80 MHz and a pulse length of, approximately, 80 fs. An LED light source illuminates the sample, and a CMOS camera (MCE-B013-UW, MighTex) is used for real-time monitoring of the TPP microprinting process (see the setup schematic in Figure S1). During the two-photon polymerization, the objective stays in place and the sample is moved according to the designed 3D trajectory with the help of two translational stages: a XYZ micro-step motor stage (MicroStage Series, MCL) coupled with a piezo stage (NanoLPS200, MCL), with motion ranges of 25 mm (XY axes) and 50 mm (Z axis) for the micro-step motor stage, and of 200 μm in X, Y and Z axes for the piezo stage. The translational stages are mounted on an inverted microscope cage (RM21 microscope, MCL). Imaging and alignment of microstructured GaAs semiconductor-based photonic chips is performed by capturing the laser reflection from the sample with an avalanche photodiode (50 μm single-photon avalanche diode—SPAD, Micro Photon Devices), synchronized with the laser via a 1 ns rise time fast photodiode (DET10A/M Si Detector, Thorlabs).

Sample preparation
The fabricated structures described in this work are fabricated in OrmoCore (Micro Resist Technology GmbH), an optical grade hybrid inorganic–organic photopolymer (n = 1.545 at λ = 830 nm). Two different types of substrates are used: glass cover slips of thickness #1.5 (160–180 μm) and GaAs semiconductor dies with microLEDs (Figure S2). To prepare the samples for TPP, the substrates are cleaned with IPA and DI water and blow dried with N_2; afterwards the polymer is drop cast onto the substrate and left to soft bake on a hotplate at 80 °C for 10 min. The sample can then be mounted on the 3D printing setup. After microprinting, the sample is left to bake on a hotplate at 130 °C for 20 min, and afterwards developed in a solution composed of two parts IPA and one part 4-methyl-2-pentanone, dissolving the liquid unexposed polymer. Finally, the developed sample is dipped in IPA for 1 min and left to dry. Sample and laser alignment details can be consulted in Figure S3.

Electro-optical characterization setup
Optical transmission characterization of the 3D waveguides, is performed using two lasers with wavelengths 635 nm and 830 nm which are coupled to lensed fibers. The light is coupled into one of the 3D waveguide's tapers through the glass substrate at an angle of approximately 15º using a microlensed optical fiber (LFM1F-1, Thorlabs). The light ouS4tcoupling from the other end of the waveguide is collected by an imaging system consisting of 16-bit monochrome sCMOS camera (CS2100M-USB, Quantalux, Thorlabs), a 4×dry objective (NA 0.1, PLN4X, Olympus), and a 3.5 mm focal distance lens (Figure a). A custom MATLAB-based image analysis tool (details in Adão et al.[34]) is used to define a square region of interest of constant area around each taper output for all taken images, and the photon counts recorded by the sCMOS camera are retrieved and converted to units of power according to the camera's quantum efficiency for the laser wavelength and then compared to the laser input power.

The interconnected system of two microLEDs and a 3D polymer waveguide was tested using a high-speed ground-signal-ground probe (ECP18-GSG-100-DP, GGB Industries Picoprobe) connected to a source meter (2280S, Keithley). One of the interconnected microLEDs is electrically pumped, setting the voltage up to 1.4 V and inducing light emission (Figure S4b). Light emission and transmission through the waveguide is captured by the same imaging system as in the optical transmission losses characterization (camera-lens-objective system).

Data availability
The data supporting this study's results is available from the corresponding author on reasonable request.

References
1. Deng, H., Lippi, G. L., Mørk, J., Wiersig, J. & Reitzenstein, S. Physics and Applications of High-β Micro- and Nanolasers. *Adv. Opt. Mater.* **9**, 2100415 (2021).

2. Romeira, B. *et al.* Brain-inspired nanophotonic spike computing: challenges and prospects. *Neuromorphic Comput. Eng.* **3**, 33001 (2023).

3. Song, S. *et al.* Recent progress of optoelectronic and all-optical neuromorphic devices: A comprehensive review of device structures, materials, and applications. *Adv. Intell. Syst.* **3**, 2000119 (2021).

4. Romeira, B., Figueiredo, J. M. L. & Javaloyes, J. NanoLEDs for energy-efficient and gigahertz-speed spike-based sub-λ neuromorphic nanophotonic computing. *Nanophotonics* **9**, 4149–4162 (2020).

5. Hejda, M. *et al.* Artificial optoelectronic spiking neuron based on a resonant tunnelling diode coupled to a vertical cavity surface emitting laser. *Nanophotonics* **12**(5), 857–867 (2023).

6. Shastri, B. J. *et al.* Spike processing with a graphene excitable laser. *Sci. Rep.* **6**, 19126 (2016).

7. Robertson, J., Hejda, M., Bueno, J. & Hurtado, A. Ultrafast optical integration and pattern classification for neuromorphic photonics based on spiking VCSEL neurons. *Sci. Rep.* **10**, 6098 (2020).

8. Winge, D. O. *et al.* Implementing an insect brain computational circuit using III–V nanowire components in a single shared waveguide optical network. *ACS Photonics* **7**, 2787–2798 (2020).

9. Jevtics, D. *et al.* Integration of semiconductor nanowire lasers with polymeric waveguide devices on a mechanically flexible substrate. *Nano Lett.* **17**, 5990–5994 (2017).

10. Mnaymneh, K. *et al.* On-chip integration of single photon sources via evanescent coupling of tapered nanowires to SiN waveguides. *Adv. Quantum Technol.* **3**, 1900021 (2020).

11. Romeira, B., Borme, J., Fonseca, H., Gaspar, J. & Nieder, J. B. Efficient light extraction in subwavelength GaAs/AlGaAs nanopillars for nanoscale light-emitting devices. *Opt. Express* **28**, 32302–32315 (2020).

12. Dolores-Calzadilla, V. *et al.* Waveguide-coupled nanopillar metal-cavity light-emitting diodes on silicon. *Nat. Commun.* **8**, 14323 (2017).

13. Dabos, G. *et al.* Neuromorphic photonic technologies and architectures: scaling opportunities and performance frontiers Invited. *Opt. Mater. Express* **12**, 2343–2367 (2022).

14. Bashir, J., Peter, E. & Sarangi, S. R. A survey of on-chip optical interconnects. *ACM Comput. Surv.* **51**, 1–34 (2019).

15. Khan, S. *et al.* Low-loss, high-bandwidth fiber-to-chip coupling using capped adiabatic tapered fibers. *APL Photonics* **5**, 056101 (2020).

16. Ishii, Y., Koike, S., Arai, Y. & Ando, Y. Ink-jet fabrication of polymer microlens for optical-I/O chip packaging. *Jpn. J. Appl. Phys.* **39**, 1490 (2000).

17. Vanmol, K. *et al.* 3D direct laser writing of microstructured optical fiber tapers on single-mode fibers for mode-field conversion. *Opt. Express* **28**, 36147–36158 (2020).

18. Yu, J. *et al.* 3D nanoprinted kinoform spiral zone plates on fiber facets for high-efficiency focused vortex beam generation. *Opt. Express* **28**, 38127–38139 (2020).

19. Marini, M. *et al.* Microlenses fabricated by two-photon laser polymerization for cell imaging with non-linear excitation microscopy. *Adv. Funct. Mater.* **33**, 2213926 (2023).

20. Osipov, V. *et al.* Fabrication of three-focal diffractive lenses by two-photon polymerization technique. *Appl. Phys. A* **107**, 525–529 (2012).

21. Hadibrata, W., Wei, H., Krishnaswamy, S. & Aydin, K. Inverse design and 3D printing of a metalens on an optical fiber tip for direct laser lithography. *Nano Lett.* **21**, 2422–2428 (2021).

22. Wei, H. *et al.* Two-photon direct laser writing of inverse-designed free-form near-infrared polarization beamsplitter. *Adv. Opt. Mater.* **7**, 1900513 (2019).

23. Moughames, J. *et al.* 3D printed multimode-splitters for photonic interconnects. *Opt. Mater. Express* **10**, 2952–2961 (2020).

24. Guo, R. *et al.* Log-pile photonic crystal fabricated by two-photon photopolymerization. *J. Opt. A Pure Appl. Opt.* **7**, 396 (2005).

25. Schell, A. W. *et al.* Three-dimensional quantum photonic elements based on single nitrogen vacancy-centres in laser-written microstructures. *Sci. Rep.* **3**, 1577 (2013).

26. Perevoznik, D. *et al.* Writing 3D waveguides with femtosecond pulses in polymers. *J. Light. Technol.* **39**, 4390–4394 (2021).

27. Panusa, G., Pu, Y., Wang, J., Moser, C. & Psaltis, D. Fabrication of sub-micron polymer waveguides through two-photon polymerization in polydimethylsiloxane. *Polymers (Basel).* **12**, 2485 (2020).

28. Moughames, J. *et al.* Three-dimensional waveguide interconnects for scalable integration of photonic neural networks. *Optica* **7**, 640–646 (2020).

29. Lindenmann, N. *et al.* Photonic wire bonding: a novel concept for chip-scale interconnects. *Opt. Express* **20**, 17667–17677 (2012).

30. Lindenmann, N. *et al.* Connecting silicon photonic circuits to multicore fibers by photonic wire bonding. *J. Light. Technol.* **33**, 755–760 (2015).

31. Billah, M. R. *et al.* Hybrid integration of silicon photonics circuits and InP lasers by photonic wire bonding. *Optica* **5**, 876–883 (2018).

32. Gao, H. *et al.* High-resolution 3D printed photonic waveguide devices. *Adv. Opt. Mater.* **8**, 2000613 (2020).

33. Baghdasaryan, T. *et al.* Design and two-photon direct laser writing of low-loss waveguides, tapers and S-bends. *J. Phys. Photonics* **3**, 45001 (2021).

34. Adão, R. M. R., Alves, T. L., Maibohm, C., Romeira, B. & Nieder, J. B. Two-photon polymerization simulation and fabrication of 3D microprinted suspended waveguides for on-chip optical interconnects. *Opt. Express* **30**, 9623–9642 (2022).

35. Marschner, D. E., Pagliano, S., Huang, P.-H. & Niklaus, F. A methodology for two-photon polymerization micro 3D printing of objects with long overhanging structures. *Addit. Manuf.* **66**, 103474 (2023).

36. Porte, X. *et al.* Direct (3+1)D laser writing of graded-index optical elements. *Optica* **8**, 1281–1287 (2021).

37. Jacob, B. *et al.* Room-temperature electroluminescence and light detection from III-V unipolar microLEDs without p-type doping. *Optica* **10**, 528–537 (2023).

38. Appaiah, K., Vishwanath, S. & Bank, S. R. Impact of fiber core diameter on dispersion and multiplexing in multimode-fiber links. *Opt. Express* **22**, 17158–17171 (2014).

Acknowledgements

Author contributions

J.B.N., B.R. and A.A. conceived the research. J.B.N. supervised the project. A.A. performed the experiments including, CAD design of 3D waveguides, polymer sample preparations, TPP printing, SEM imaging optical characterization of the samples, simulations, and data analysis. T.L.A. optimized the TPP sample processing protocol used in this study. C.M. optimized femtosecond laser calibration, tuning and setup alignment. B.J. and

B.R. provided the microLED samples and operated the setup for electro-optical characterization of 3D waveguide interconnected microLEDs. A.A. and J.B.N. wrote the manuscript with the input from all authors.

Competing interests
The authors declare no competing interests.

Additional information
Supplementary Information The online version contains supplementary material available at https://doi.org/10.1038/s41598-024-69522-0.

Correspondence and requests for materials should be addressed to J.B.N.

Reprints and permissions information is available at www.nature.com/reprints.

Publisher's note Springer Nature remains neutral with regard to jurisdictional claims in published maps and institutional affiliations.